

Fabrication, polarization, and characterization of PVDF matrix composites for integrated structural load sensing

Ghazaleh Haghashtiani and Michael A Greminger

Dept. of Mechanical and Industrial Engineering, University of Minnesota Duluth, 1305 Ordean Court, Duluth, MN 55812, USA

E-mail: mgremin@umn.edu

Received 1 October 2014, revised 27 January 2015

Accepted for publication 15 February 2015

Published 10 March 2015



Abstract

The focus of this work is to evaluate a new carbon fiber reinforced composite structure with integrated sensing capabilities. In this composite structure, the typical matrix material used for carbon fiber reinforced composites is replaced with the thermoplastic polyvinylidene difluoride (PVDF). Since PVDF has piezoelectric properties, it enables the structure to be used for integrated load sensing. In addition, the electrical conductivity property of the carbon fabric is harnessed to form the electrodes of the integrated sensor. In order to prevent the carbon fiber electrodes from shorting to each other, a thin Kevlar fabric layer is placed between the two carbon fiber electrode layers as a dielectric. The optimal polarization parameters were determined using a design of experiments approach. Once polarized, the samples were then used in compression and tensile tests to determine the effective d_{33} and d_{31} piezoelectric coefficients. The degree of polarization of the PVDF material was determined by relating the effective d_{33} coefficient of the composite to the achieved d_{33} of the PVDF component of the composite using a closed form expression. Using this approach, it was shown that optimal polarization of the composite material results in a PVDF component d_{33} of 3.2 pC N^{-1} . Moreover, the Young's modulus of the composite structure has been characterized.

Keywords: carbon fiber reinforced composites, PVDF, smart composites, structural health monitoring

(Some figures may appear in colour only in the online journal)

1. Introduction

In order to examine the safety and durability of structures, and to detect any damage or defect that can lead to catastrophic failures, structures need to be examined through a process called structural health monitoring (SHM). For this purpose, different non-destructive evaluation techniques can be adopted such as visual inspections, ultrasonic methods, eddy currents, x-ray radiography, thermography, or shearography [1, 2]. However, all of these techniques have one of two limitations. They either do not allow the online monitoring of the structure during its operation, or they just allow the assessment of specific locations on the structure. Moreover, in the case of composite structures, the SHM process becomes

even more complicated due to their different failure modes and the potential for inherent imperfections during the fabrication process [3, 4].

A technology that has evolved in the recent years is the use of smart composite materials for the purpose of SHM. Smart materials have specific properties that enable them to react to external factors such as thermal, magnetic, electrical, or mechanical stimuli [5]. Consequently, these types of materials have a wide range of applications for sensing and actuating purposes. Embedding these smart materials in composite structures has resulted in self-sensing structures. As suggested in the literature [6, 7], this self-sensing capability of smart composite structures is analogous to the nervous system of the human body.

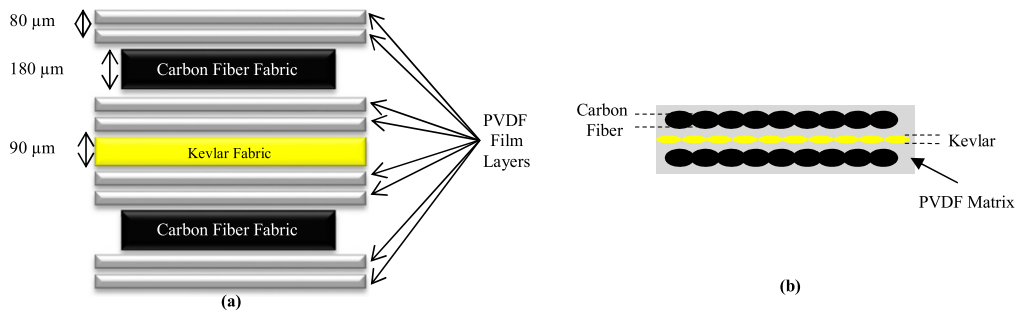


Figure 1. The stack-up of reinforcement fabrics and PVDF film layers before melting (a) and after melting (b).

In this study, a new carbon fiber-reinforced polymer (CFRP) composite structure has been proposed. In this structure, the typical matrix material used in CFRPs has been replaced with the piezoelectric material polyvinylidene difluoride (PVDF). The piezoelectric properties of PVDF will enable the proposed composite structure to have integrated sensing capabilities for SHM.

1.1. Related works

Several efforts have been made to develop self-sensing composite structures. For instance, Abot *et al* stitched a carbon nanotube (CNT) thread as a sensor into carbon/epoxy and glass/epoxy composite structures and used electrochemical impedance spectroscopy to monitor the changes in the resistance of the sensor thread and, as a result, detect strain and defects such as delamination [8]. Loyola *et al* spray-deposited a multi-walled carbon nanotube and PVDF (MWCNT–PVDF) thin film on a glass fiber mat and then used it in a glass fiber-reinforced polymer. They implemented electrical impedance tomography (EIT) to detect damage in the composite structure [9, 10]. EIT is a method used for spatial imaging in which an array of electrodes is attached around the surface of the object being studied. Electric current is applied between a pair of the attached electrodes, while the resulting electric potential is recorded using the other remaining electrodes. Moreover, several works [11–14] have focused on embedding optical fiber Bragg grating sensors within the composite structure to monitor the structure during the curing process and its operation.

The main difference between the smart composite structure proposed in this article and the previous works is that no external material is required to be inserted or woven into the composite structure. Thus, the fabrication process for the proposed material is the same as traditional thermoplastic matrix composites. In addition, the original properties of the reinforcement fabrics are not affected.

2. Research methodology

The research methodology used consists of three stages: (1) sample fabrication; (2) sample polarization; and (3) tensile testing to quantify the degree of polarization. The required procedures for each stage are described in the following sections.

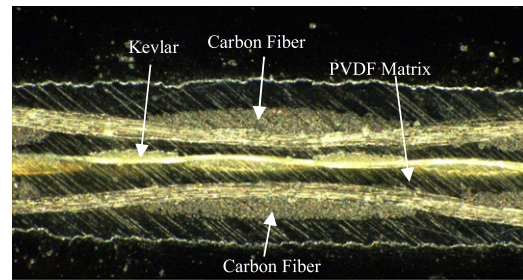


Figure 2. Cross-section of the prepared samples.

2.1. Sample preparation

The smart composite samples use two layers of carbon fiber to form the electrodes of the piezoelectric sensors. In order to prevent the two carbon fiber layers from shorting to each other, a Kevlar layer is placed between them as a dielectric barrier. Kevlar fibers have mechanical properties near those of carbon fiber materials [15], so there is little sacrifice to the mechanical properties of the overall structure. In order to achieve high electric field between the two carbon fiber layers when the structure is under stress, it is desirable to make the Kevlar layer as thin as possible, which also decreases the Kevlar layer's overall impact on the mechanical properties of the composite structure. Two layers of 80 μm thick PVDF film are placed in between each of the fabric layers. Figures 1(a) and (b) show a schematic of the composite structure before and after melt curing. Figure 2 shows a cross-section of one of the actual samples. The samples were made by applying a 7 kPa pressure and heating the PVDF film to its melting temperature using an oven. Figure 3 shows the actual test samples before and after melt curing. The duration of heating was 4 h and the temperature of oven was set to 200 $^{\circ}\text{C}$. The capacitance of the 100 \times 80 mm samples was measured to be between 800 and 900 pF.

For performing the tensile test, the samples must be placed between two grips. Using the samples shown in figure 3(b) is not appropriate for this purpose because the grips will cause a compression on the sample that will affect the results of the tensile test. In order to prevent this error, the above sample structure was further extended by adding two layers of Kevlar on each side of the sample, along with two layers of PVDF on the top and bottom as shown in figure 3(c). These additional layers of Kevlar were bonded to

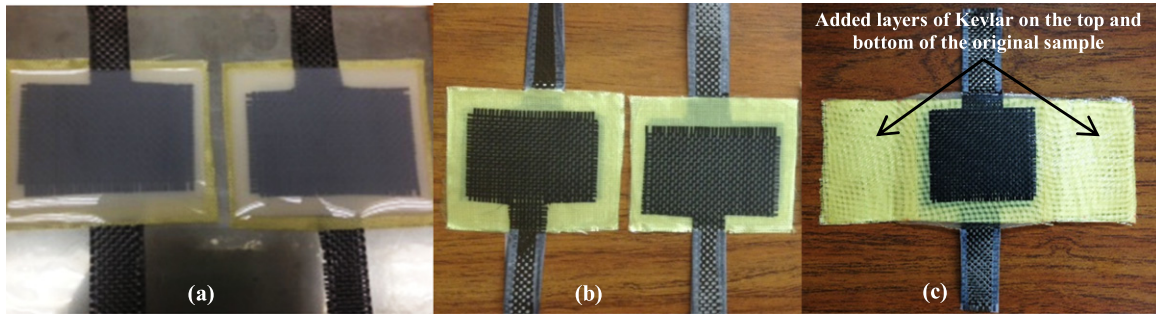


Figure 3. Original samples before melting the PVDF films (a), original samples after melting the PVDF films (b), and extended sample for tensile testing (c).

the structure during the melt cure process. With this new structure, the attached layers of Kevlar will be placed between the grips so no pressure is applied to the carbon fiber electrodes during the tensile test.

2.2. Poling PVDF

In order for the smart composite structure to generate responses due to an applied load, the PVDF material must be polarized to align the dipole moments of its crystalline structure. The crystalline structure of the PVDF film will determine the polarization properties of the film. There are four possible crystalline forms of the PVDF polymer: the alpha, beta, gamma, and delta phases [16]. Only the beta, gamma, and delta phases can be polarized. However, the alpha phase can also be polarized by applying a large electric field, which will convert the alpha phase to the delta phase [16]. The processing conditions of the PVDF film determine the dominant crystalline phase. When the PVDF film layers in the composite samples are melted and solidified, the dominant phase is the alpha crystalline phase [17]. Since the alpha phase is the dominant phase upon solidification, an electric field must be applied to convert the alpha phase to the delta phase and to align the dipoles for the proposed smart composite structures. Existing research shows that an electric field of around 125 MV m^{-1} is required to fully polarize a predominately alpha phase PVDF film [18]. However, a higher piezoelectric coefficient can be attained by polarizing a beta phase film since the beta crystal phase has a greater dipole moment than the delta phase [19]. One of the most common means mentioned in the literature to achieve a predominately beta phase PVDF film is to stretch the film mechanically to many times its original length [20]. A second method to transition from an alpha phase film to a beta phase film is to apply a very high electric field on the order of 500 MV m^{-1} [18]. A third method mentioned in the literature to achieve a predominately beta phase PVDF film is to cure the film under high pressure [21]. Finally, the copolymers of PVDF containing trifluoroethylene (TrFE) or tetrafluoroethylene can be added to the film to encourage the formation of the beta phase [22].

For the purpose of this study, the most common polarization method of stretching is not applicable because the



Figure 4. Experimental setup for tensile test.

carbon fiber and Kevlar reinforcements are very stiff and prevent strain greater than a few percent. Moreover, previous works have required very high fields to polarize a predominately alpha phase film. However, in this study due to the inevitable imperfections of the composite structure, high fields cannot be applied because it will cause dielectric breakdown. Consequently, this study will focus on polarizing the PVDF films by applying relatively lower electric fields for a specific duration of time while heating the samples since both duration and temperature of poling have been shown to influence the degree of polarization [23]. In order to find the optimal poling condition, a design of experiments (DOE) was performed that will be discussed in detail in section 3.

2.2.1. Tensile test. After polarization the response of the samples to applied tensile loads was observed using an MTS material testing system. A cyclic force with the amplitude of 130 N was applied to the samples at the frequency of 1 Hz. The charge generated in the sample due to the applied tension is extracted as the output. The setup used for the tensile test is shown in figures 4 and 5.

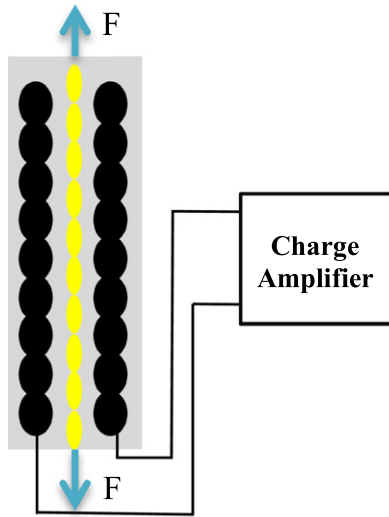


Figure 5. Schematic of the applied load F to the samples during the tensile test.

Table 1. Design of experiment factors and their levels.

Factor	Low level	High level
Temperature	50 °C	150 °C
Voltage	1000 V	2000 V
Duration of poling	5 min	20 min

3. Poling optimization

3.1. Experimental procedure

In order to find the optimal condition for poling the smart composite structure and to also investigate the effects of different factors on sample’s polarization, a 2^3 full factorial DOE was used. The three factors that were studied in the DOE were temperature, voltage, and duration of poling. These factors and their levels are shown in table 1.

In each of the runs, a constant voltage was applied to the sample for a specific period of time while the sample was placed on a hot plate at the specified temperature. After the poling step, the response of the samples was monitored in the tensile test and the ratio of the charge developed in the sample to the applied force was calculated (Charge/Force or Q/F). For the reliability of the results, each of the experiments was replicated two times, resulting in 16 total runs. The results obtained from the DOE were analyzed using Minitab 16 software.

3.2. Main effects

The main effects plots depict the effect of the change in each of the factors on the response. The main effects plots of temperature, voltage, and duration of poling are shown in figure 6. As it can be seen in figure 6, changing voltage and duration of poling from the low level to their high level causes an increase to the response of the sample. On the other

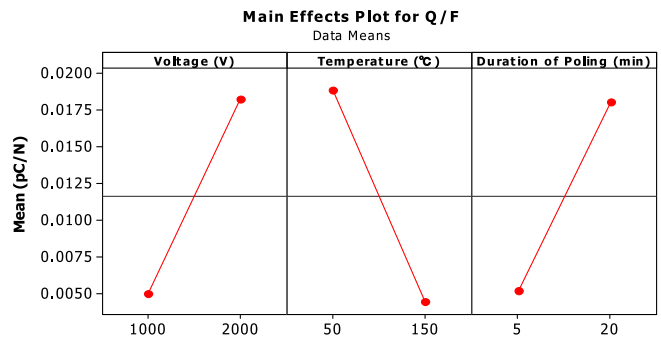


Figure 6. Main effect plots for Q/F .

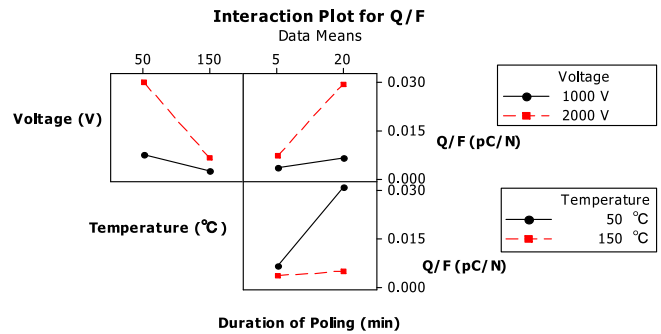


Figure 7. Interaction plot for Q/F .

hand, changing the temperature from low level to high decreases the response.

3.3. Interaction plot

Figure 7 illustrates the interactions between each pair of factors. Also, for each pair, it shows the sensitivity of the response to the changes of one factor at a specified level of the other. The fact that each pair of lines has different slopes signifies that all the factors have significant interactions. According to the voltage and temperature interaction plot, the response has a higher value at 50 °C than 150 °C for both levels of voltage. Also, the response is more sensitive to the changes of temperature at the high level of voltage. The voltage and duration of poling interaction plot suggests that the response for poling at the duration of 20 min is higher than 5 min for both levels of voltage and it is more sensitive to the changes of duration of poling at the high level of voltage. Finally, the temperature and duration of poling interaction plot shows that poling the samples for a longer duration (20 min) causes a higher response than shorter duration (5 min) for both levels of temperature. In addition, the response is more sensitive to the changes in the duration of poling at the low level of temperature.

3.4. Finding the optimal temperature

According to the above results, samples generate higher response when they have been poled at the higher levels of voltage and duration of poling and at the lower level of temperature. However, since there was actually a negative influence of temperature on polarization, it was postulated

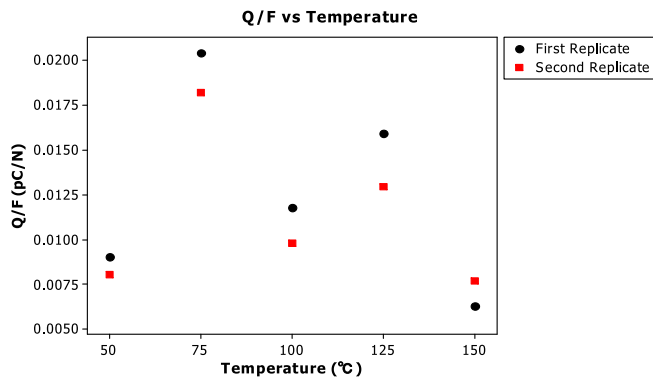


Figure 8. Q/F ratio as a function of temperature.

that the samples could potentially have a higher response at a poling temperature between 50 °C and 150 °C due to a non-linearity in the impact of temperature. In order to find that optimal temperature, a single factor experiment was performed for different temperatures between 50 °C and 150 °C ($T=75$ °C, 100 °C, and 125 °C) at the high levels of voltage and duration of poling. For the integrity of the experiment, each of the runs was replicated two times. The results, as shown in figure 8, suggest that the samples generate the highest response at 75 °C. Moreover, samples that are poled at 150 °C have the lowest response. These results confirm that there is a nonlinear relationship between the degree of polarization and the polarization temperature. This nonlinear relationship has been observed in the literature as well [24].

4. Sample characterization

The smart composite samples were characterized for both their mechanical and piezoelectric properties as described in the following sections.

4.1. Mechanical characterization

For the mechanical characterization, the Young's modulus was investigated as a measure for stiffness of the proposed composite structure. For this purpose, a tensile test was performed on the samples using the same MTS machine that was used for the polarization DOE. In addition, an extensometer was attached to it in order to monitor the strain developed in the sample due to an applied tensile load. Figure 9 shows the setup of this experiment.

This experiment was also performed on separate samples using only carbon fiber and Kevlar reinforcements in order to find the relative Young's modulus for each of these materials, which was used in the calculations of the piezoelectric constants discussed in section 4.2. See figure 10 for the composition of these samples before melt curing.

4.1.1. Young's modulus of the smart composite structure.

Figure 11 illustrates the stress-strain plot of the composite sample obtained from the tensile test. As it can be seen in figure 11, the strain-stress plot is not linear at the beginning of

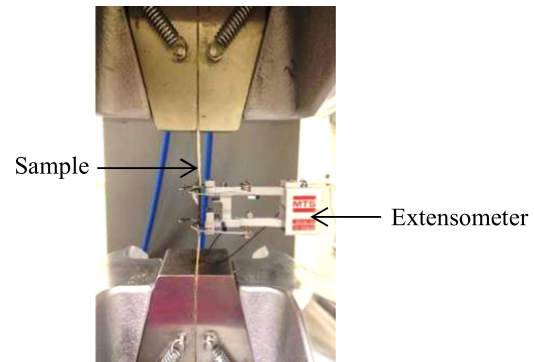


Figure 9. Test setup for finding the Young's modulus.

loading. This is because the composite samples were not perfectly flat after fabrication. In order to make sure that there is no bending occurring for the data used to calculate Young's modulus, only the last portion of the curve was used and the extensometer was placed at both sides of the sample, which confirmed the absence of bending. The last section of the strain-stress plot (as shown in figure 11) becomes linear once the initial curvature of the samples is straightened out. For the credibility of the results, two different samples were tested. The Young's modulus for each sample was calculated by averaging the slopes of loading and unloading plots for the two sides of each sample. The final Young's modulus was calculated by averaging the Young's modulus of the two tested samples, which resulted in a modulus of $E = 16.4$ Gpa for the composite structure. Table 2 summarizes the obtained results.

4.1.2. Young's moduli of carbon fiber and kevlar materials.

Figures 12 and 13 show the stress-strain plots of carbon fiber and Kevlar individual samples, respectively. For the integrity of results, the last sections of the stress-strain plots were taken into consideration for calculating the Young's modulus. Two different samples were tested for each of the fiber materials. For each tested sample, the Young's modulus was found by averaging the slope of the loading and unloading plots. The Young's modulus of each fiber reinforced composite was calculated by averaging the modulus of their two tested samples. Table 3 summarizes the Young moduli and the volume fractions of fiber material (ν_f) and matrix material (ν_m) in the tested structures.

The results show that the Young's modulus of the Kevlar composite is 65.6% of the modulus of carbon fiber composite. This ratio would be used in section 4.2.1 for finding the amount of applied force on the middle layer of the composite structure for the calculation of the effective d_{31} coefficient.

4.2. Piezoelectric characterization

In order to characterize the piezoelectric properties of the composite structure, the effective d_{31} and d_{33} coefficients were investigated. Prior to performing the required experiments for finding these coefficients, the frequency influence on the sample's response was studied in order to find an optimal frequency for performing the tests. For this purpose,

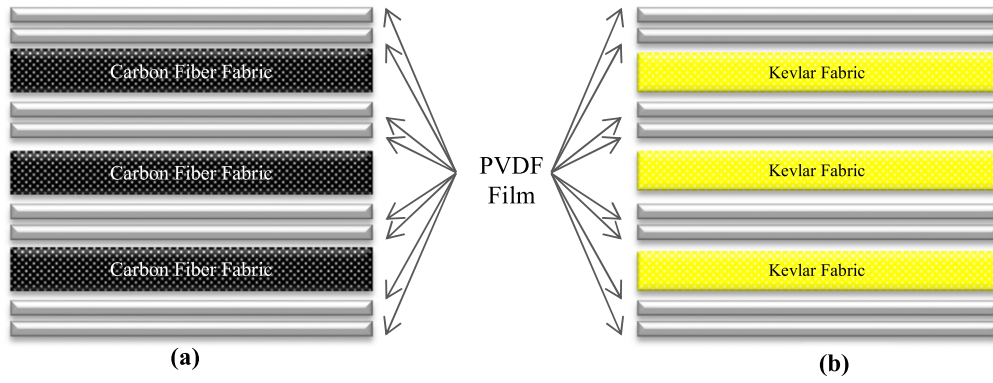


Figure 10. Sample structure used for finding the Young's modulus for individual reinforcement materials: (a) carbon fiber, (b) Kevlar.

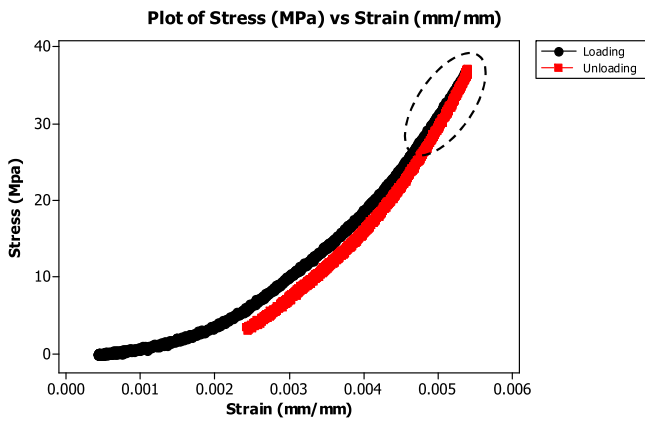


Figure 11. Stress-strain plot for smart composite structure.

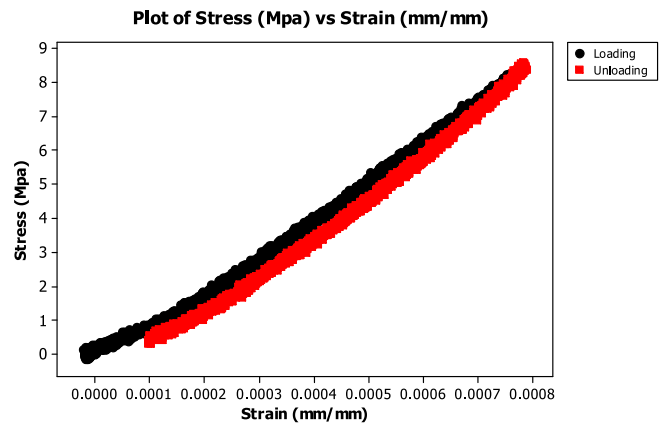


Figure 12. Stress-strain plot for a carbon fiber/PVDF composite.

Table 2. Results of Young's modulus for the proposed composite structure.

		E (Gpa)	
Sample 1	Side 1	Loading	16.540
		Unloading	19.609
		Average	18.075
	Side 2	Loading	13.724
		Unloading	17.468
Average		15.596	
Average of both sides (E_1)		16.836	
Sample 2	Side 1	Loading	13.197
		Unloading	16.874
		Average	15.036
	Side 2	Loading	14.992
		Unloading	19.012
Average		17.002	
Average of both sides (E_2)		16.019	
Composite structure	Avg (E_1, E_2)	16.428	

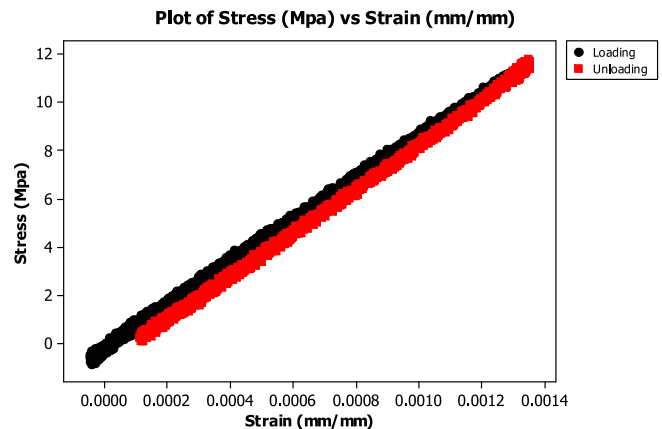


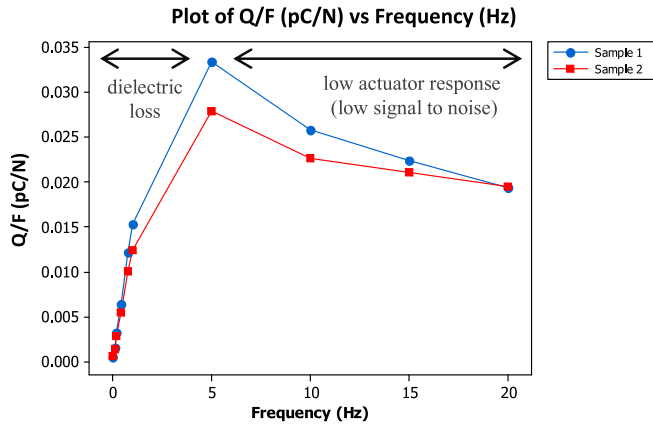
Figure 13. Stress-strain plot for a Kevlar/PVDF composite.

the sample's response was quantified as the ratio of the charge developed in the sample to the applied force at 10 different frequencies from 0.01 to 20 Hz in a tensile test. The experiment was performed for two different samples. The results are shown in figure 14.

As it can be seen in figure 14, at lower frequencies, the response of the samples is low due to dielectric loss. At higher frequencies, there is low actuator response due to the mechanical limitations of the tensile testing machine. In other words, the equipment's noise dominates the actual signal in higher frequencies. From the frequencies that were tested,

Table 3. Results of Young moduli for carbon fiber/PVDF and Kevlar/PVDF samples.

		Carbon fiber/PVDF	Kevlar/PVDF
ν_f		0.360	0.173
ν_m		0.640	0.827
Sample 1	Loading	11.717 Gpa	8.538 Gpa
	Unloading	16.352 Gpa	10.155 Gpa
	Average (E_1)	14.035 Gpa	9.347 Gpa
Sample 2	Loading	10.564 Gpa	5.724 Gpa
	Unloading	13.297 Gpa	9.653 Gpa
	Average (E_2)	11.931 Gpa	7.688 Gpa
Composite	Avg(E_1, E_2)	12.983 Gpa	8.518 Gpa

**Figure 14.** Composite sample's response at different frequencies in tensile test.

5 Hz was chosen for performing the tensile and compression tests in order to measure the d_{31} and d_{33} coefficients, respectively.

4.2.1. d_{31} coefficient. For calculating the d_{31} coefficient, a tensile test was performed on the composite samples. The setup used for the tensile test is shown in figure 15(a). A cyclic force with the amplitude of about 15 N was applied to the sample at the frequency of 5 Hz. The charge generated in the sample due to the applied tension was extracted as the output. In order to find the effective d_{31} coefficient, the force that is applied to the middle layer of the composite structure (between the two carbon fiber electrode layers) needs to be known. For this purpose, the two carbon fiber layers and the layer between them (consisting of Kevlar and PVDF matrix) are assumed to be three parallel springs (see figure 15(b)). Knowing that parallel springs have equal displacements, the following equations can be written:

$$\delta_{CF} = \delta_{K+PVDF} \rightarrow \frac{F_{CF}L_{CF}}{E_{CF}A_{CF}} = \frac{F_{K+PVDF}L_{K+PVDF}}{E_{K+PVDF}A_{K+PVDF}}, \quad (1)$$

$$F_{tot} = 2F_{CF} + F_{K+PVDF}, \quad (2)$$

where δ , F , L , E , and A are respectively the displacement, force, length, Young's modulus, and area of each layer as indicated by the given subscript (CF: carbon fiber; K: Kevlar; K+PVDF: the middle layer between two carbon fiber electrodes). (1) and (2), along with the ratio of Kevlar to carbon fiber elastic modulus found in section 4.1.2, can be used to solve for F_{CF} (force applied on each carbon fiber layer) and F_{K+PVDF} (force applied on the middle layer consisting of Kevlar and PVDF matrix). Knowing the force applied to the middle layer, the stress (σ_{K+PVDF}) can be determined ($\sigma_{K+PVDF} = \frac{F_{K+PVDF}}{A_{K+PVDF}}$, where A_{K+PVDF} is the cross-sectional area of the middle layer). Finally, the effective d_{31} can be calculated as follows:

$$(d_{31})_{eff} = \frac{Q/A_{CF,electrode}}{\sigma_{K+PVDF}}, \quad (3)$$

where Q is the charge developed in the samples during the tensile test, A is the area of the carbon fiber electrodes, and σ_{K+PVDF} is the stress applied to the middle layer of the sample.

Figure 16 shows the plot of the force applied to the samples and the charge developed in them during the tensile test. According to figure 16, the amplitude of the applied tensile force was 15.9 N and the amplitude of the charge developed in the samples was 0.48 pC.

Using (1) and (2), the force applied on the middle layer was found to be 5.6 N and the stress on this layer was 0.452 Mpa. Finally, knowing the stress on the middle layer and the charge developed on the sample, the $(d_{31})_{eff}$ was calculated using (3) as $(d_{31})_{eff} = 1.6 e^{-4} \frac{pC \cdot m^{-2}}{N \cdot m^{-2}}$.

The obtained value for $(d_{31})_{eff}$ was lower than expected. Three possible reasons for this result have been investigated. First, due to the lower tensile modulus of PVDF compared to Kevlar and Carbon fiber, only a small fraction of total force (~6%) is being transmitted to the PVDF layers in the middle. Because of this small amount of force, the stress developed in the PVDF is low. Second, it is possible that the PVDF layers have not been fully polarized. In order to examine this point, and to determine the degree of polarization of the PVDF layers, the measurement of effective d_{33} coefficient is discussed in the next section. Using an existing analytical formulation for the effective d_{33} for piezoelectric composite materials, the d_{33} coefficient of PVDF layers can be found. Comparing this value with the existing d_{33} values of PVDF in literature, the degree of polarization of PVDF layers in the composite structure can be investigated. Finally, the electrical impact of the Kevlar dielectric layer could contribute to the low effective d_{31} coefficient.

4.2.2. d_{33} coefficient. In order to find the d_{33} coefficient, a compression test was performed on the samples. The setup used for the compression test is shown in figure 17(a). A cyclic compression force with the amplitude of 180 N was applied to the sample at the frequency of 5 Hz. The charge generated in the sample due to the applied compression was extracted as the output.

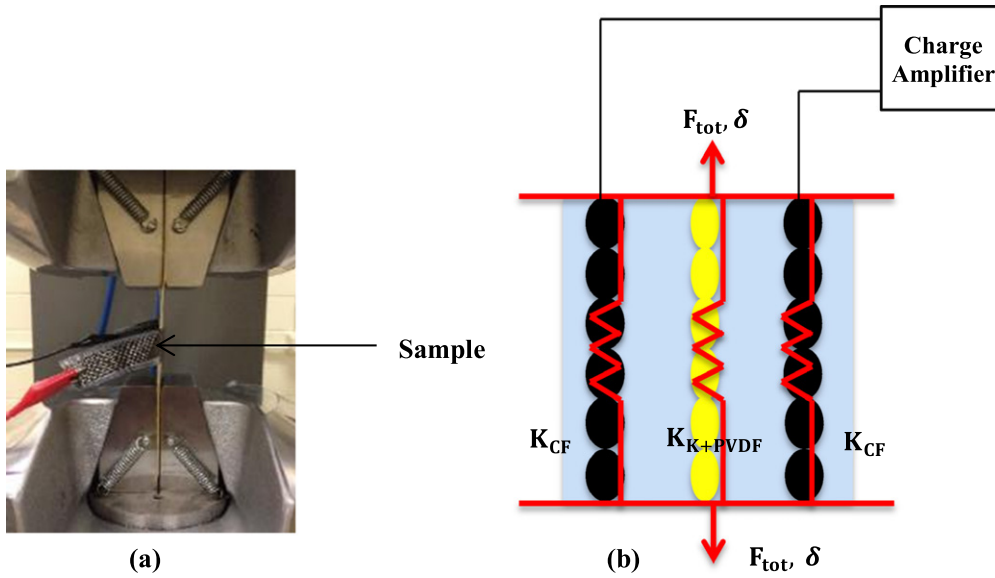


Figure 15. Experimental setup (a) and schematic of the assumed parallel springs (b) for finding the effective d_{31} coefficient.

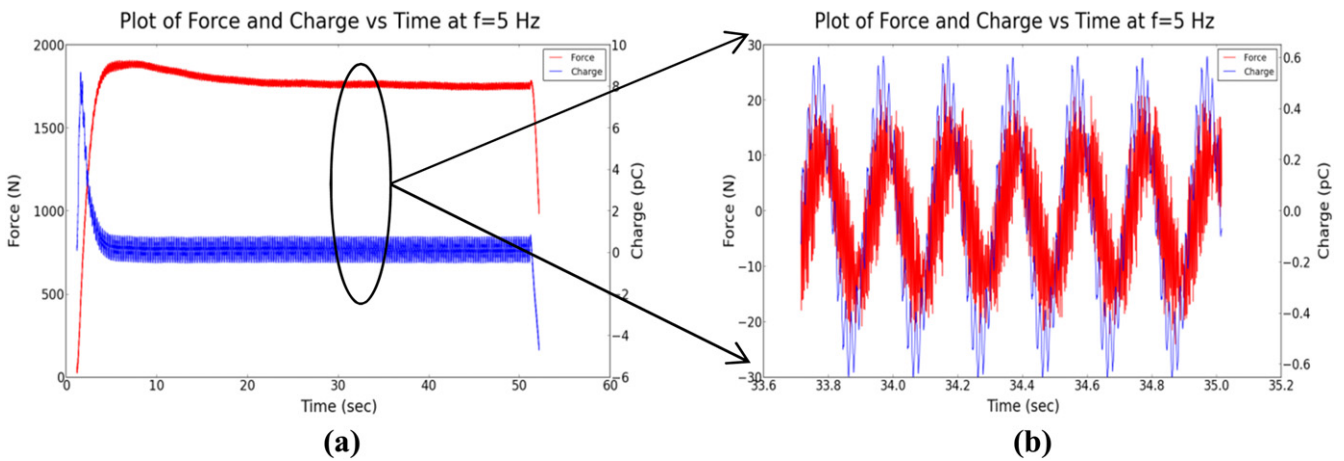


Figure 16. Plots of force and charge versus time in tensile test: complete plot (a) and detail plot with the dc component removed (b).

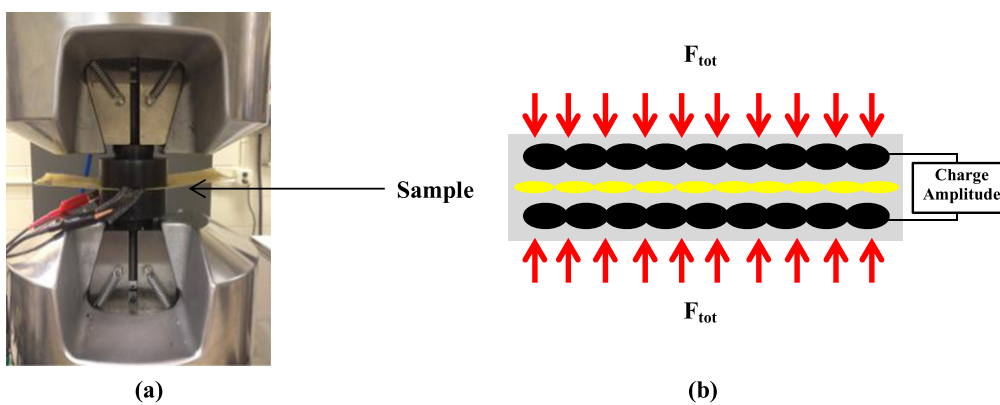


Figure 17. Experimental setup (a) and schematic of the applied load (b) for finding the effective d_{33} coefficient.

As it can be seen in figure 17(b), in the compression case, the stress applied to the effective layer (the middle layer consisting of Kevlar and PVDF) is equal to the total stress. Consequently, the experimental value of $(d_{33})_{eff}$ can be calculated as follows:

$$(d_{33})_{eff} = \frac{Q/A_{CF,electrode}}{\sigma_{K+PVDF}} \tag{4}$$

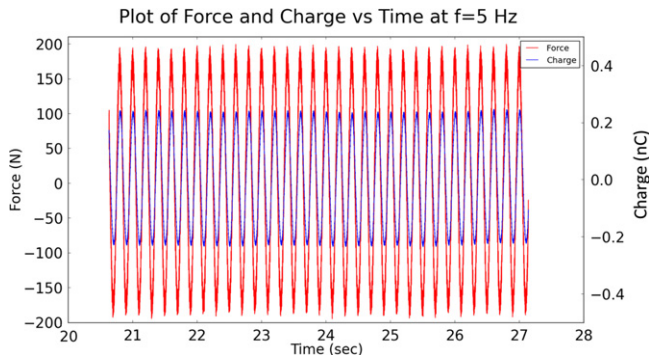


Figure 18. Plot of force and charge versus time in compression test.

The experimental value of $(d_{33})_{\text{eff}}$ can then equated to the following equation, which represents the formulation for effective d_{33} coefficient for a piezoelectric composite with continuous fiber inclusions [25]:

$$(d_{33})_{\text{eff}} = [v_{\text{PVDF}}(d_{33})_{\text{PVDF}}(\epsilon_{33})_{\text{Kevlar}} + v_{\text{Kevlar}}(d_{33})_{\text{Kevlar}} \times (\epsilon_{33})_{\text{PVDF}}] / [v_{\text{PVDF}}(\epsilon_{33})_{\text{Kevlar}} + v_{\text{Kevlar}}(\epsilon_{33})_{\text{PVDF}}], \quad (5)$$

where v_{PVDF} and v_{Kevlar} signify the volume fraction of PVDF and Kevlar in the effective layer, and $(\epsilon_{33})_{\text{PVDF}}$ and $(\epsilon_{33})_{\text{Kevlar}}$ represent the permittivity constant of PVDF and Kevlar, respectively. Equation (5) can be solved for $(d_{33})_{\text{PVDF}}$. The results will be compared to the literature values for $(d_{33})_{\text{PVDF}}$ in order to quantify the degree of polarization of the samples.

Figure 18 shows the plot of the force applied to the samples and the charge developed in them due to the applied force in the compression test. As it can be seen in figure 18, the amplitude of the applied compressive force was 176 N and the amplitude of the charge developed in the samples was 0.235 nC.

As mentioned above, the amount of the force applied to the middle layer between the carbon fiber layers is equal to the total force (176 N). Consequently, the amount of applied stress on the middle layer is 0.043 Mpa. Then, using (4), the effective d_{33} coefficient was found to be $(d_{33})_{\text{eff}} = 1.289 \frac{\text{pC m}^{-2}}{\text{N m}^{-2}}$. Next, the $(d_{33})_{\text{eff}}$ was substituted into (5) and the equation was solved for $(d_{33})_{\text{PVDF}}$, which yields $(d_{33})_{\text{PVDF}} = 3.25 \frac{\text{pC m}^{-2}}{\text{N m}^{-2}}$.

Finally, the achieved d_{33} coefficients were compared to the values in the literature as shown in table 4.

The obtained result for the piezoelectric coefficients suggests that some degree of polarization has been achieved and it confirms the sensing capability of the proposed composite structure. However, the comparison of the experimental values of the piezoelectric constants with values in literature shows that there is still potential for the enhancement of the degree of polarization to achieve improved sensitivity.

5. Conclusions

5.1. Summary

This study introduced the concept of a new carbon fiber-reinforced polymer composite and the preliminary results of its development. The main difference between this proposed composite and other CFRP composites is that the common polymers typically used for the matrix material have been replaced with the piezoelectric polymer PVDF. The piezoelectricity of PVDF as the matrix material, along with the electrical conductivity of carbon fibers as the reinforcement material, enable this composite to have integrated force sensing capabilities that can be used for *in situ* SHM of CFRP structures.

The results of the polarization DOE showed that high levels of voltage and duration of polarization have a positive impact on the charge generated by samples when exposed to an applied load. However, the effect of temperature was nonlinear. Given the temperatures that were tested in this study, poling at 75 °C showed the highest response.

Next, the proposed composite structure was characterized from both the mechanical and piezoelectric perspectives. For the mechanical characterization, the Young's modulus of the composite was investigated as a measure of its stiffness. The results showed an average Young's modulus of 16.4 Gpa for the composite. For the purpose of piezoelectric characterization, the piezoelectric coefficients d_{31} and d_{33} were studied in tensile and compression tests, respectively. The experiments led to effective piezoelectric coefficients of $(d_{31})_{\text{eff}} = 1.6 e^{-4} \frac{\text{pC m}^{-2}}{\text{N m}^{-2}}$ and $(d_{33})_{\text{eff}} = 1.3 \frac{\text{pC m}^{-2}}{\text{N m}^{-2}}$ for the proposed composite structure. These results confirmed the potential capability of this composite structure to act as an integrated sensor. In addition, the comparison of these results with literature values suggests that there is capacity for further enhancements in the degree of polarization.

5.2. Future work

Based on the results achieved for the piezoelectric coefficients, the future work for this project involves improving the degree of polarization. For this purpose, two methods will be investigated. One approach is to melt cure the composite sample under an increased pressure in order to reduce the thickness of the middle Kevlar/PVDF layer, which will increase the electric field during poling. A second method is to apply the poling voltage during the melt curing of the sample. This is possible since the carbon fiber layers are present during the melt curing process. The poling voltage will continue to be applied as the PVDF is cooled and solidifies. Recent work in a 3D printing application has suggested that PVDF films can be successfully poled with a field applied during solidification [30].

In addition, the practical application of this composite structure as a sensor for failure detection and *in situ* SHM will be investigated. For this purpose, a meshed structure can be used to localize the stress measurement by measuring the appropriate pair of carbon fiber electrodes as shown in

Table 4. Comparison of the obtained values for d_{33} coefficients with values in literature.

		d_{33} ($\frac{pC}{N}$)	Reference
Bulk PVDF	Experimental	3.247	—
	Theoretical	13–28	[26]
PVDF in other forms	Proposed composite structure (carbon fiber-Kevlar/PVDF)	1.289	—
	PZT/PVDF-HFP 50/50 vol%	25	[27]
	PVDF-HFP 90:10	3	[27]
	PVDF-TrFE	22.1	[28]
	30% BaTiO ₃ (whiskers)/PVDF(normal) with poling field 3 KV mm ⁻¹	13.7	[29]
	30% BaTiO ₃ (powder)/PVDF with poling field 3 KV mm ⁻¹	4.4	[29]

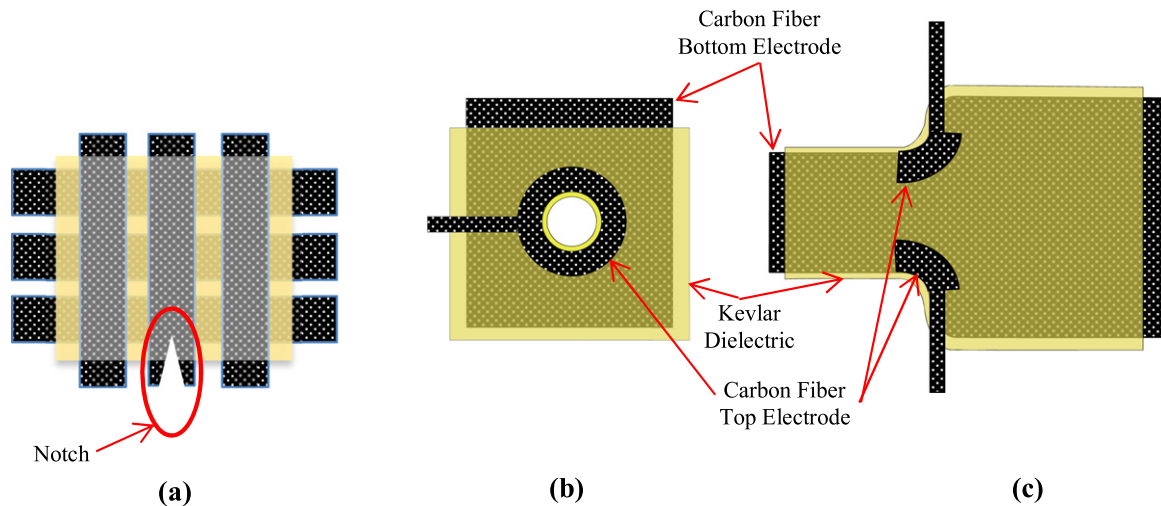
**Figure 19.** Proposed composite test structures to evaluate the smart composite material for damage detection by using a grid structure (a) or by locating the carbon fiber electrodes in areas of stress concentrations (b) and (c).

figure 19(a). In order to evaluate the potential of the composite for failure detection, a notch will be introduced into one of the elements of the mesh. This sample can then be placed under a cyclical load to quantify the response of each of the cells as the crack propagates across the sample. Alternatively, for a structural application, the carbon fiber electrodes can be placed at stress concentration locations as shown in figures 19(b) and (c).

Acknowledgments

This work was supported by the Swenson College of Science and Engineering of the University of Minnesota Duluth.

References

- [1] Staszewski W, Boller C and Tomlinson G R 2004 *Health Monitoring of Aerospace Structures: Smart Sensor Technologies and Signal Processing* (New York: Wiley)
- [2] Giurgiutiu V and Soutis C 2012 Enhanced composites integrity through structural health monitoring *Appl. Compos. Mater.* **19** 813–29
- [3] Kessler S S, Spearing S M and Soutis C 2002 Damage detection in composite materials using Lamb wave methods *Smart Mater. Struct.* **11** 269
- [4] Lissenden C J and Rose J L 2008 Structural health monitoring of composite laminates through ultrasonic guided wave beam forming *NATO Applied Vehicle Technology Symp. on Military Platform Ensured Availability Proc.*
- [5] Srinivasan A V and McFarland D M 2001 *Smart Structures: Analysis and Design* (Cambridge: Cambridge University Press)
- [6] Akhras G 2000 Smart materials and smart systems for the future *Can. Mil. J.* **1** 25–31
- [7] Cao W, Cudney H H and Waser R 1999 Smart materials and structures *Proc. Natl Acad. Sci.* **96** 8330–1
- [8] Abot J L, Song Y, Vatsavaya M S, Medikonda S, Kier Z, Jayasinghe C, Rooy N, Shanov V N and Schulz M J 2010 Delamination detection with carbon nanotube thread in self-sensing composite materials *Compos. Sci. Technol.* **70** 1113–9
- [9] Loyola B R, Briggs T M, Arronche L, Loh K J, La Saponara V, O'Bryan G and Skinner J L 2013 Detection of spatially distributed damage in fiber-reinforced polymer composites *Struct. Health Monit.* **12** 225–39
- [10] Tallman T N, Gungor S, Wang K W and Bakis C E 2015 Damage detection via electrical impedance tomography in glass fiber/epoxy laminates with carbon black filler *Struct. Health Monit.* **14** 100–9
- [11] Guemes J A and Menéndez J M 2002 Response of Bragg grating fiber-optic sensors when embedded in composite laminates *Compos. Sci. Technol.* **62** 959–66

- [12] Kuang K, Kenny R, Whelan M P, Cantwell W J and Chalker P R 2001 Embedded fibre Bragg grating sensors in advanced composite materials *Compos. Sci. Technol.* **61** 1379–87
- [13] Leng J and Asundi A 2003 Structural health monitoring of smart composite materials by using EFPI and FBG sensors *Sensors Actuators A* **103** 330–40
- [14] Murukeshan V M, Chan P Y, Ong L S and Seah L K 2000 Cure monitoring of smart composites using fiber Bragg grating based embedded sensors *Sensors Actuators A* **79** 153–61
- [15] Laszlo G S S and Kollar P 2009 *Mechanics of Composite Structures* (Cambridge: Cambridge University Press)
- [16] Bloomfield P E 1988 Production of ferroelectric oriented PVDF films *J. Plast. Film Sheeting* **4** 123–9
- [17] Lovinger A J 1982 *Developments in Crystalline Polymers* (Amsterdam: Springer) pp 195–273
- [18] Davis G T, McKinney J E, Broadhurst M G and Roth S 1978 Electric-field-induced phase changes in poly(vinylidene fluoride) *J. Appl. Phys.* **49** 4998–5002
- [19] Kepler R G and Anderson R A 1992 Ferroelectric polymers *Adv. Phys.* **41** 1–57
- [20] Sajkiewicz P, Wasiak A and Goćłowski Z 1999 Phase transitions during stretching of poly(vinylidene fluoride) *Eur. Polym. J.* **35** 423–9
- [21] Ohigashi H and Hattori T 1995 Improvement of piezoelectric properties of poly(vinylidene fluoride) and its copolymers by crystallization under high pressures *Ferroelectrics* **171** 11–32
- [22] Dargaville T R, Celina M C, Elliott J M, Chaplya P M, Jones G D, Mowery D M, Assink R A, Clough R L and Martin J W 2005 *Characterization, Performance and Optimization of PVDF as a Piezoelectric Film for Advanced Space Mirror Concepts* Sandia National Laboratories
- [23] Furukawa T, Date J and Fukada E 1980 Hysteresis phenomena in polyvinylidene fluoride under high electric field *J. Appl. Phys.* **51** 1135–41
- [24] Nilsson E, Lund A, Jonasson C, Johansson C and Hagström B 2013 Poling and characterization of piezoelectric polymer fibers for use in textile sensors *Sensors Actuators A* **477–86**
- [25] Neelakanta P S 1995 Piezoelectric composite materials *Handbook of Electromagnetic Materials: Monolithic and Composite Versions and Their Applications* 1st edn (Boca Raton: CRC Press) pp 293–305
- [26] Ramadan K S, Sameoto D and Evoy S 2014 A review of piezoelectric polymers as functional materials for electromechanical transducers *Smart Mater. Struct.* **23** 033001
- [27] Malmonge L F, Malmonge J A and Sakamoto W K 2003 Study of pyroelectric activity of PZT/PVDF-HFP composite *Mater. Res.* **6** 469–73
- [28] Zeng R, Kwok K W, Chan H L W and Choy C L 2002 Longitudinal and transverse piezoelectric coefficients of lead zirconate titanate/vinylidene fluoride-trifluoroethylene composites with different polarization states *J. Appl. Phys.* **92** 2674
- [29] Chen L F, Hong Y P, Chen X J, Wu Q L, Huang Q J and Luo X T 2004 Preparation and properties of polymer matrix piezoelectric composites containing aligned BaTiO₃ whiskers *J. Mater. Sci.* **39** 2997–3001
- [30] Lee C and Tarbutton J A 2014 Electric poling-assisted additive manufacturing process for PVDF polymer-based piezoelectric device applications *Smart Mater. Struct.* **23** 095044